A New Technique to Detect Ocular Pathologies Based on Electrical Measurement Implemented on Programmable Logic

Mariela I. Bellotti, Damián Dellavale, and Fabián J. Bonetto

***Abstract*—We developed a technique that detects superficial ocular pathologies based on the measurement of electrical impedance spectra. The sensor used is a small microelectrode made of platinum insulated from a cylindrical counterelectrode built of surgical stainless steel. The sensor has the shape of a truncated cone made of acrylic with dimensions identical to that of a standard Goldman prism. The sensor is applied to normal and pathological subject eyes with a constant force provided by a commercial tonometer. The circuit is closed through the lacrimal layer and the epithelial and endothelial cells. We measure the electrical impedance with a programmable logic device in which we implemented all the significant functions. These are the synthesis of the seventeen sines for the excitation, one lock-in, and delta–sigma modulators for the digital-to-analog converter and analog-to-digital converter requirements. A simple analog circuit filters the output, implements a voltage divider, and acts as current limiter in order not to damage the cells. We convert the measurements to resistance and capacitance as a function of frequencies. Consistent results are obtained for left and right eyes of the normal subjects. Significant differences are detected between the results for normal eyes and pathological eyes.**

***Index Terms*—Electrical impedance, lock-in, ocular pathologies.**

I. Introduction

MEDICAL APPLICATIONS that involve electrical impedance measurements are, in general, inexpensive and effective.

Over the last years, a substantial knowledge advancement has been produced about the ocular surface and the associated tissue in humans [1], [2]. The electron transport through the cells and the tight junctions are related to the permeability of the ions, macromolecules, and water on the ocular surface. Measuring the electrical impedance spectra, we can obtain an indirect estimation of the cell behavior.

Giaever and Keese pioneered an electrical impedance method coupled with a model to estimate cell monolayer characteristics *in vitro* [3], [4]. Our group proposed an alternative model based on a mean field approach [5]. Both methods are based on the electrical impedance measurement using lock-ins [6], [7].

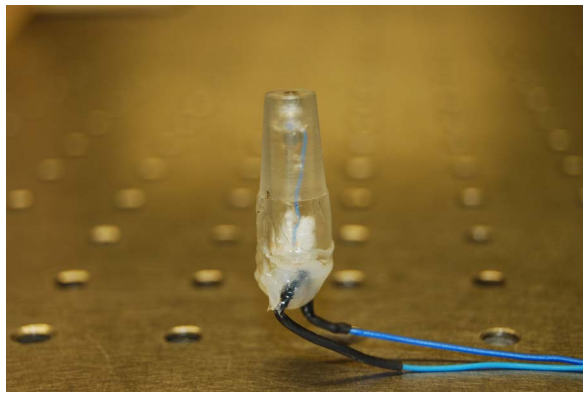

Fig. 1. Shows a picture of the sensor used in this work.

We have developed new lock-ins based on digital signal processors and field-programmable gate arrays (FPGAs) optimized for the *in vivo* measurements corresponding to those in this paper [6]–[12].

We have used the knowledge base that we built using *in vitro* [13] and *in vivo* (rabbits) [14] experiments to develop and test a whole system that we used with human eyes.

For that purpose, we have designed, built, and tested a sensor (Fig. 1) with an associated electronic system (Fig. 2) that generated electrical impedance measurements of the ocular surface to detect pathologies in human eyes.

The optimum diameter of the active electrode was the result of *in vitro* experiments performed with variable radius microelectrodes in the range of 30–500 μm [13]. A prototype was first tested on rabbits, where we generate an ulcer using alcohol, and therefore, these became our pathological eyes. The measurements on these rabbit eyes were compared with measurements in rabbit normal eyes to establish the differences in signals between normal and pathological eyes [14].

In this paper, we present the electrical impedance spectra of a platinum microelectrode in contact with a subject ocular surface and show the difference between the measurements of a normal eye and a pathological eye (*in vivo*).

II. Methods and Materials

A. Sensor

The sensor (Fig. 1) itself is a 300-μm platinum wire surrounded by a Pyrex tube. The glass tube is converted into

Manuscript received November 22, 2011; revised April 17, 2012; accepted May 13, 2012. Date of publication September 19, 2012; date of current version November 15, 2012. The Associate Editor coordinating the review process for this paper was Dr. Domenico Grimaldi.

M. I. Bellotti is with the Laboratorio de Cavitación y Biotecnología, Instituto Balseiro/Centro Atómico Bariloche, 8400 San Carlos de Bariloche, Argentina.

D. Dellavale and F. J. Bonetto are with the Laboratorio de Cavitación y Biotecnología, Instituto Balseiro/Centro Atómico Bariloche, 8400 San Carlos de Bariloche, Argentina (e-mail: fabian.bonetto@gmail.com).

Color versions of one or more of the figures in this paper are available online at http://ieeexplore.ieee.org.

Digital Object Identifier 10.1109/TIM.2012.2210458

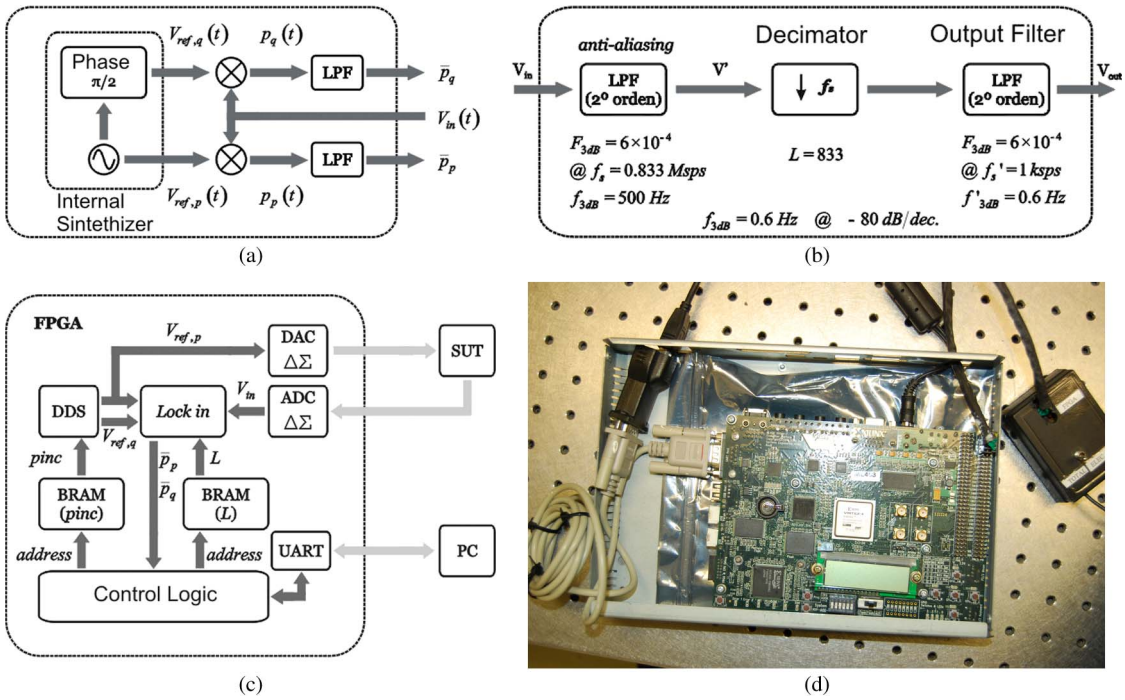

Fig. 2. (a) Basic functions of the LIA. (b) Details of the LPF showing the decimation strategy that allows the use of 32-bit arithmetic libraries to program the FPGA. (c) All the modules programmed in the FPGA, the SUT, and the PC that control the FPGA and acquire the data. (d) Picture of the whole system.

a micropipette using a puller. The micropipette is cut with a diamond pencil at a location such that the inner diameter of the glass is close and slightly larger than 300 μm. The platinum is inserted in the micropipette, and the system is flamed with a small oxyacetylene flame (used in standard glass work) until the micropipette collapse around the platinum wire. The extra platinum is cut. The glass is the primary insulator for the wire, and it is biocompatible as well as the platinum wire. The glass–Pt arrangement is inserted in a 2-mm inner diameter surgical stainless steel tube (also biocompatible). The empty space is filled with acrylic dissolved in chloroform. After drying, only the acrylic (also biocompatible) remains in the system. This package is inserted in an acrylic truncated cone with the same dimensions as a standard Goldman prism to be used in commercial tonometers. The platinum wire (live or positive electrical contact) and the stainless steel tube (ground or counterelectrode) are connected with AWG30 wire to pins for adequate connections to the sensing circuitry.

B. Electrolyte Cells

The circuit between the platinum wire and the stainless steel counterelectrode is closed with the lacrimal layers, the epithelial cells, and the endothelial cells. The area of the Pt microelectrode is much smaller than the counterelectrode area. Thus, if we only have physiological saline on the sensor (Fig. 3), the electrical impedance is determined by the conditions close to the Pt microelectrode. Three discrete electrical elements should be considered: 1) The double-layer Helmholtz capacitance $C_{\rm dl}$; 2) the faradaic (charge transfer) resistance R_F; and 3) the solution resistance R_s. The elements 1) and 2) occur in distances on the order of 1 nm, so they are mainly surface effects. The capacitance $C_{\rm dl}$ is proportional to the microelectrode area A, and the resistance R_F is inversely proportional to the microelectrode area A. The resistance R_s is the constriction resistance, and it is proportional to the solution electrical resistivity (and inversely proportional to the square root of the microelectrode area A). The epithelial cells (Fig. 3) have tight junction (barrier function) that obstructs the electrical current flow, so one expects that that significantly affects the measurements. We have performed Electric Cell-substrate Impedance Sensing (ECIS) experiments in a conjunctive line cell IOBA-NHC (Instituto OftalmoBiología Aplicada—Normal Human Conjunctiva) that show this effect *in vitro* [13] and in rabbits *in vivo* [14].

C. Electronic System Implementation

Electrical impedance spectra are typically measured effectively with either network analyzers or lock-in amplifiers (LIAs). Network analyzers are preferred for high-frequency low-noise applications. For relatively high-noise low-frequency applications such as those present in this work, LIAs are preferred. The basic components and operations of a LIA are shown in Fig. 1(a). A sinusoidal signal, internal to the LIA, low distortion, and variable frequency are generated $(V_{{\rm REF},p}(t))$. This signal is fed to the system under study (SUT) that is assumed to be linear. The output of the SUT $(V_{\rm in}(t))$ is the only input of the LIA. The voltages $V_{\rm in}(t)$ and $V_{\rm REF}(t)$ are phase sensitive detected (PSD), and the output is low-pass filtered to produce the in-phase result p_p. Similarly, the $V_{\rm REF}(t)$ is phase shifted $\pi/2$ to produce a cosine $[V_{{\rm REF}q}(t)]$. This value is also PSD with $V_{\rm in}$ and low-pass filtered producing the out-of-phase output p_q. In our application, $V_{\rm in}(t)$ is the voltage across the sensor electrodes produced by a sinusoidal current obtained from $V_{\rm REF}(t)$ as we explain as follows.

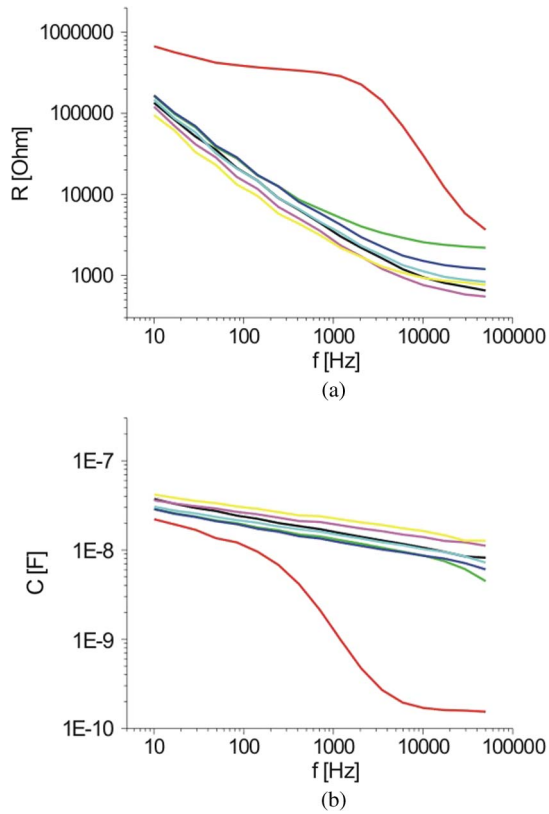

Fig. 3. (a) Resistance and (b) capacitance for the sensor using the following fluids–solutions: (Red curve) Distilled water; (black curve) physiological solution of 300 mOsm/L; (green curve) NaCl solutions with concentrations of 2, (blue curve) 4, and (cyan curve) 8 mg/mL; and (magenta and yellow) tears of two subjects.

We programmed the basic functions of the LIA in an FPGA programmable logic device (Model Virtex, brand name Xilinx). These are the following: 1) the synthesis of the reference signal; 2) the phase shift of 90° for the reference signal; 3) the phase-sensitive detector; 4) the low-pass filters (LPFs) that are identical for the p and q channels and have programmable cutoff frequencies (integration times); 5) the digital-to-analog converter (DAC) (to generate the excitation voltage sine wave); and 6) the analog-to-digital converter (ADC) (to digitize the voltage $V_{\rm in}(t)$). For the DAC and ADC functions, we use delta–sigma converters.

For an efficient performance, the design of the LPF is critical. In what follows, we describe the design rationale and performance of the LPF first. It is a well-known fact that the LIA measurement quality depends on the stability and the absence of oscillatory behavior of the filter. Also important for our design is to keep the filter coefficients not so different to take advantage of standard 32-bit Very High Speed Integrated Circuits Hardware Description Language arithmetic libraries.

A schematic of the LPF is shown in Fig. 1(b). It consists of two second-order Chebyshev filters in cascade with a decimator block inserted between the two filters. The two LPFs shown in Fig. 1(a) are identical and are shown in Fig. 1(b); thus, we do not distinguish from now on between p_p and p_q, and we call the filter input just $p_p(t)$. In Fig. 1(b), $p_p(t)$ is sampled at $f_s = 0.833$ Msamples/s, and this filter acts as antialiasing filter with cutoff frequency of $F_{-3\ \rm dB} = 610^{-4}$ cycles/sample, with an overall (time domain) cutoff frequency of $f_{-3\ \rm dB} = 500$ Hz. The coefficients of the IIR filter differ in six orders of magnitude and can be represented by 32-bit fixed point arithmetic without stability or quantization problems according to our simulations.

Discrete IIR LPFs with very low cutoff frequencies (therefore suitable for LIAs) have coefficients that differ in many orders of magnitude. An effective strategy to reduce the number of bit requirements is to have a decimator that downsamples a factor L in frequency of the output of the antialiasing filter.

For the case of Fig. 2, the Nyquist frequency is 1 kHz, and therefore, the maximum allowed $L = 833$. With only changes in L in the range of 1–833, we can control the overall cutoff frequency of the LPF. Finally, a second-order IIR Chebyshev filter is inserted with a discrete domain cutoff frequency of $F_{-3\ \rm dB} = 610^{-4}$ cycles/sample, the sampling frequency being $f_s' = 1$ ksample/s and the cutoff frequency being $f_{-3\ \rm dB}' = 0.6$ Hz in the time domain. The overall performance corresponds to a fourth-order IIR Chebyshev filter with a minimum cutoff frequency in the time domain $f_{\rm LPF} = 0.6$ Hz and a rolloff of -80 dB/dec. Fig. 1(c) shows the whole system with the indication that the L value is programmable $(1 < L < 833)$.

Sine and Cosine Generation: The system allows the generation of frequency scans through the programming of the Direct Digital Synthesis block. The block produces the synthesis of the in-phase and out-of-phase components (sine and cosine) with low harmonic distortion using the phase-dithering technique. This technique reduces quantization errors produced by the phase accumulator. Two block RAMs are used. In one memory, we store the phase increment (pinc, 26 bits), and in the other, we store the L values (10 bits). We do not change the coefficients of the IIR filter. Instead, as it was explained, we vary the L value.

Finally, the in-phase voltages and the out-of-phase voltages are read by a computer through a serial port. The computer also begins the frequency scan.

The analog filter was a simple resistance–capacitance LPF that was used with the delta–sigma DAC. In a previous work, we used as the current limiter an $R_L = 1$ MΩ resistor in series with the reference signal. This strategy degrades the response for relatively high frequency. In this paper, we used a voltage divider and an $R_L = 50$ kΩ to improve the frequency response of the whole system.

III. Performance

In this section, we characterize the system (sensor and electronics) under controlled conditions. We placed the sensor vertically in a holder with an O-ring that fitted the truncated face of the acrylic cone forming a small vessel. With the help of a Pipetor, we added 50 μL of different liquids, and we measure the spectral response of the sensor. The resistance R and the capacitance C as functions of the excitation frequency f are shown in Fig. 3(a) and (b), respectively. The fluids/solution used were as follows: distilled water (red curve), physiological solution of 300 mOsm/L (black curve), NaCl solutions with concentrations 2 (green curve), 4 (blue curve), and 8 mg/mL (cyan curve), and tears of two subjects (magenta and yellow). Assuming that the theory for the double-layer capacitance of the gold-electrode/electrolyte interphase is applicable, we can

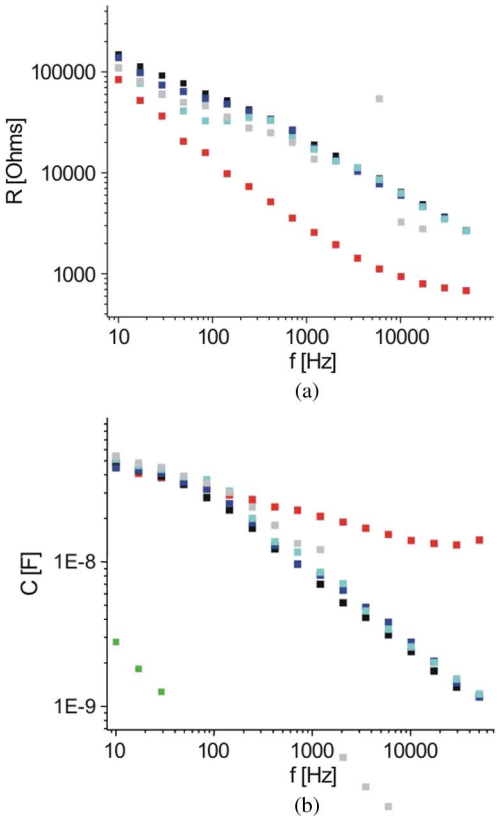

Fig. 4. Shows the (a) resistance and (b) capacitance spectral response for a subject normal cornea with black symbols (applied pressure of 14 mmHg) and the sensor response immersed in physiological saline with red symbols. We measure with different pressures. With the tonometer pressure set at 14, 10, 20, and 14 mmHg, we obtained the black, light blue, blue, and gray solid squares. With the (green squares) bare sensor, resistance was very high and out of scale. The three gray squares that deviate from the trend correspond to the moment in which the eye of the volunteer was removed from the sensor.

compute the double-layer capacitance value C_{dl}, the faradaic (charge resistance) resistance R_F, and the solution resistance R_s [15].

The curves in Fig. 3 depend on C_{dl}, R_F, and R_s. The measured resistance is equal to the solution resistance when the frequency goes to infinity. The measured resistance is equal to the faradaic resistance when the frequency tends to zero. The former limit is not reached in our experiments except for the distilled water curve (red curve). For the other fluids/solutions shown in Fig. 3, the measured low frequencies were not low enough to reach this asymptotic limit. We see that the physiological saline has resistance spectra close to the tears (they correspond to normal eyes). This suggest that the osmolarity of the physiological saline is close to the tears' osmolarity (i.e., close to 300 mOsm/L).

IV. Results

Fig. 4 shows the impedance spectral response for a patient with normal eye with the sensor located in the cornea. As a reference, we also show the sensor response immersed in physiological saline with red square symbols.

The electrical impedance spectra were measured with the sensor applied to the patient's right eye. The result of this measurement is shown in Fig. 4(a) and (b) with black squares.

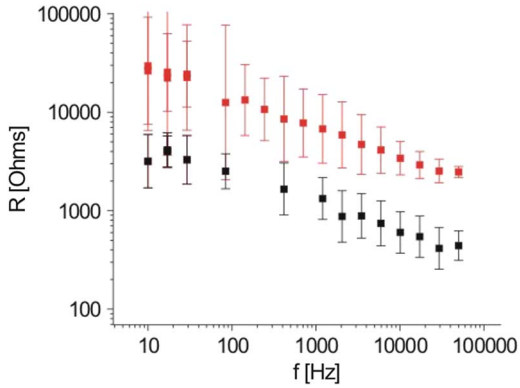

Fig. 5. Shows measurements comparing the electrical resistance in the conjunctiva of normal eyes with measurements of a pathological eye corresponding to a subject that suffers from a severe case of cicatricial pemphigoid.

We can observe that the the resistance is larger than the naked (with physiological saline) sensor and the curvature in the log–log plot changes from positive to negative. For very low frequencies and for very high frequencies, the contrast between the two curves is smaller than that in the intermediate frequency range.

We measure with different pressures set on the tonometer, and these are 14, 20, 10, and 14 mmHg.

The frequency sweep took 80 s for each measurement. With the tonometer pressure set at 14, 20, 10, and 14 mmHg, we get the black, light blue, blue, and gray solid squares, respectively.

With the (green squares) bare sensor, resistance is very high (they were out of the scale as shown in the graph). The resistances were on the order of 1 MΩ for low frequencies and 0.1 MΩ for high frequencies. The three gray squares that deviate from the trend correspond to the moment in which the eye of the volunteer was separated from the device (results are similar to the bare sensor).

The anesthesia used for these measurements was proparacaine hydrochloride 0.5%, and we waited 1 min before starting the measurements.

In Fig. 4(b), we can observe that the capacitance of the eye measurements is very close to the physiological saline for low and intermediate frequencies. For higher frequencies, there exist a significant contrast, and the higher the frequency, the larger the contrast. From an extensive medical evaluation, we know that this eye corresponds to a normal eye.

Fig. 5 shows with black solid squares the logarithmic average of the normal eye spectral electrical resistance for several subjects. In the measurements, we located the sensor on the conjunctiva. We also show the standard deviation in the measurements with error bars. Each subject was measured a single time in the right and left eyes. The total number of eye measurements in the curve is $n = 12$. The error bars are an indication of the variabilities between the right and left eyes and the differences between subjects. The subjects were extensively tested before and were identified as normal.

Fig. 5 shows in red solid squares the pathological eyes corresponding to a subject that suffers from a severe case of ocular cicatricial pemphigoid [16]. We measured both eyes of this subject four times each. That makes a total of $n = 8$ nonindependent measurements.

We can observe that the resistance results are a factor of ten different between the normal eyes and the pathological eyes. For normal eyes in the frequency range of $f = 1000$ Hz–10 kHz (midrange frequencies), there was a significant contrast between normal eyes and eyes with the disease. In fact, the pathological eyes show resistances that are much higher than those of the normal eyes (note that the scale is logarithmic).

A specialist performed a slit-lamp visual inspection of the ocular (corneal and conjunctival) surface for each subject using fluorescein before and after the measurements verifying that no damage on the ocular surface occurred.

V. Conclusion

The ECIS is a noninvasive technique that allows the monitoring of cellular resistance and capacitance as a function of frequency in real time.

In this paper, we have shown that the device (built entirely in our laboratory) can be used in human eyes without producing damage on the ocular surface.

We observed very consistent and repetitive results in a given patient and between different normal patients.

The applied pressure to the eye did not affect the results significantly. The applied pressures used in this experiment were the same as those commonly used by ophthalmologic devices for the measurement of ocular pressure.

The times involved in the measurement, that is to say, the times that the sensor is in contact with the eye, are adequate for clinical use.

The implementation of an optimized algorithm for the digital signal processing based on lock-in technique allowed us to make these measurements.

Acknowledgment

The authors would like to thank A. Berra, M. Berra, V. Paolantonio, and M. I. Márquez.

References

[1] C. G. Begley, R. L. Chalmers, and G. L. Mitchell, "Characterization of ocular surface symptoms from optometric practices in North America," *Cornea*, vol. 20, no. 6, pp. 610–618, Aug. 2001.

[2] M. A. Lemp, C. Baudouin, and J. Baum, "The definition and classification of dry eye disease: Report of the Definition and Classification Subcommittee of the International Dry Eye Workshop," *Ocul. Surf.*, vol. 5, no. 2, pp. 75–92, Apr. 2007.

[3] I. Giaever and C. R. Keese, "Monitoring fibroblast behavior in tissue culture with an applied electric field," *Proc. Natl. Acad. Sci. USA*, vol. 81, no. 12, pp. 3761–3764, Jun. 1984.

[4] I. Giaever and C. R. Keese, "Toxic? Cells can tell," *Chemtech*, vol. 22, pp. 116–125, Feb. 1992.

[5] E. Urdapilleta, M. I. Bellotti, and F. J. Bonetto, "Impedance analysis of cultured cells: A mean-field electrical response model for electric cell-substrate impedance sensing technique," *Phys. Rev. E.*, vol. 74, no. 4, pp. 041908-1–041908-11, Oct. 2006.

[6] M. O. Sonnaillon, R. Urteaga, and A. Bonetto, "High-frequency digital lock-in amplifier using random sampling," *IEEE Trans. Instrum. Meas.*, vol. 57, no. 3, pp. 616–621, Mar. 2008

[7] M. O. Sonnaillon and F. J. Bonetto, "A low cost, high performance, DSP-based lock-in amplifier capable of measuring multiple frequency sweeps simultaneously," *Rev. Sci. Instrum.*, vol. 76, no. 2, pp. 024703-1–024703-7, Feb. 2005.

[8] D. Dellavale, M. O. Sonnaillon, and F. J. Bonetto, "FPGA based multi-harmonic control system for single bubble sonoluminescence," in *Proc. 4th SPL*, Bariloche, Argentina, 2008, pp. 269–272.

[9] M. O. Sonnaillon and F. J. Bonetto, "FPGA implementation of a phase locked loop based on random sampling," in *Proc. 3rd Southern Conf. Program. Logic*, Mar del Plata, Argentina, 2007, pp. 1–6.

[10] M. Ordoñez, M. O. Sonnaillon, M. T. Iqbal, J. E. Quaicoe, and F. J. Bonetto, "An embedded DSP-based frequency response analyzer for fuel cells monitoring and characterization," in *Proc. IEEE PESC*, 2006, pp. 1–7.

[11] M. O. Sonnaillon, R. Urteaga, F. J. Bonetto, and M. Ordoñez, "Implementation of a high-frequency digital lock-in amplifier," in *Proc. 18th CCECE*, Saskatoon, Saskatchewan, Canadá, May 2005, pp. 1229–1232.

[12] J. M. Iriarte Muñoz, D. Dellavale, M. O. Sonnaillon, and F. J. Bonetto, "Real-time particle image velocimetry based on FPGA technology," in *Proc. SPL*, 2009, pp. 147–152.

[13] M. I. Bellotti, W. Bast, A. Berra, and F. J. Bonetto, "Effects of osmolarity on human epithelial conjunctival cells using an electrical technique," *Graefe's Arch. Clin. Exp. Ophthalmol.*, vol. 249, no. 12, pp. 1875–1882, Dec. 2011.

[14] M. I. Bellotti, W. Bast, A. Berra, and F. J. Bonetto, "A new experimental device to diagnose eye ulcers using a multispectral electrical impedance technique combined with a lock-in amplifier," *Rev. Sci. Instrum.*, vol. 82, no. 7, pp. 074303-1–074303-5, Jul. 2011.

[15] D. A. Borkholder, "Cell based biosensors using microelectrodes," Ph.D. dissertation, Stanford Univ., Stanford, CA, Nov., 1998.

[16] C. S. Foster, "Cicatricial pemphigoid," *Trans. Am. Ophthalmol. Soc.*, vol. 84, pp. 527–663, 1986.

Mariela I. Bellotti was born in Cordoba, Argentina. She received the B.Sc. degree in biochemistry from the Universidad Nacional de Cordoba, Cordoba, in 1998 and the Ph.D. degree in medicine from the Universidad de Buenos Aires, Buenos Aires, Argentina, in 2010.

She is currently an Assistant Professor with the Universidad Nacional del Comahue, San Carlos de Bariloche, Argentina. She is also a Researcher with the Laboratorio de Cavitación y Biotecnología, Instituto Balseiro/Centro Atómico Bariloche, San Carlos de Bariloche. Her interests include the use of electric cell-substrate impedance sensing to detect pathologies.

Damián Dellavale was born in Río Ceballos, Argentina, in 1975. He received the degree in electronic engineering from the Universidad Tecnológica Nacional, Córdoba, Argentina, in 2003 and the Ph.D. degree in engineering from the Instituto Balseiro, San Carlos de Bariloche, Argentina, in 2012.

Since 2008, he has been a Professor in charge of assignments of electronics with the Instituto Balseiro/Centro Atómico Bariloche, San Carlos de Bariloche, where he is currently a Postdoctoral Fellow with the Laboratorio de Cavitación y Biotecnología. His research interests include algorithms and concurrent architectures for signal processing, field-programmable gate array technology, control theory, electrical bioimpedance sensing, and sonoluminescence.

Fabián J. Bonetto was born in Maria Juana, Santa Fe, Argentina. He received the degree in nuclear engineering and a Ph.D. degree in nuclear engineering degree from Instituto Balseiro, San Carlos de Bariloche, Argentina, in 1987 and 1990, respectively.

He was an Assistant Professor with Rensselaer Polytechnic Institute, Troy, NY. He is currently a Full Professor with Instituto Balseiro/Centro Atómico Bariloche, San Carlos de Bariloche, and a Researcher with the Consejo Nacional de Investigaciones Científicas y Técnicas, Buenos Aires, Argentina, and with the Comision Nacional de Energia Atomica, San Carlos de Bariloche. His interests include biotechnological applications and the study of sonoluminescence.